

# Cognitive Orthogonal Precoder for Two-tiered Networks Deployment

Marco Maso, Leonardo S. Cardoso, Mérouane Debbah, Lorenzo Vangelista

▶ **To cite this version:**

Marco Maso, Leonardo S. Cardoso, Mérouane Debbah, Lorenzo Vangelista. Cognitive Orthogonal Precoder for Two-tiered Networks Deployment. IEEE Journal on Selected Areas in Communications, 2013, pp.2338 - 2348. 10.1109/JSAC.2013.131108 . hal-00923423

**HAL Id: hal-00923423**

**https://centralesupelec.hal.science/hal-00923423**

Submitted on 2 Jan 2014

**HAL** is a multi-disciplinary open access archive for the deposit and dissemination of scientific research documents, whether they are published or not. The documents may come from teaching and research institutions in France or abroad, or from public or private research centers.

L'archive ouverte pluridisciplinaire **HAL**, est destinée au dépôt et à la diffusion de documents scientifiques de niveau recherche, publiés ou non, émanant des établissements d'enseignement et de recherche français ou étrangers, des laboratoires publics ou privés.

# Cognitive Orthogonal Precoder for Two-tiered Networks Deployment

Marco Maso[⋆,◇], Leonardo S. Cardoso[†], Mérouane Debbah[⋆] and Lorenzo Vangelista[◇]

⋆ Alcatel-Lucent Chair - SUPÉLEC, Gif-sur-Yvette, France

◇ Department of Information Engineering, University of Padova, Italy

† INSA - Lyon, France

{marco.maso, merouane.debbah}@supelec.fr, leonardo.sampaio-cardoso@inria.fr, lorenzo.vangelista@unipd.it

**Abstract**

In this work, we consider a two-tiered network, where a tier of cognitive small base stations is deployed inside the coverage area of a preexisting macro-cell. The cross-tier interference caused by a complete bandwidth sharing is managed by introducing a new orthogonal precoder based mechanism, implemented by the small base stations. This technique, called multi-user Vandermonde-subspace division multiplexing (MU-VFDM), allows to cancel the interference generated by several cognitive small base stations towards legacy macro cell receivers, without any cooperation between the two tiers. The achievable sum rate of the small-cell network, satisfying the interference cancelation requirement, is evaluated for perfect/imperfect channel state information at the transmitter (CSIT). Simulation results for MU-VFDM show a comparable performance to that of state-of-the-art dirty paper coding technique, for the case of a dense cellular layout. Finally, we propose a comparison between MU-VFDM and a standard spectrum partitioning strategy, and show promising gains in terms of achievable rate for the two-tiered network w.r.t. the traditional bandwidth management approach.

**Index Terms**

Interference cancelation, overlay cognitive network, complete sharing, small cells, linear precoding

# I. INTRODUCTION

Recent academic and industry trends are pointing towards the adoption of a new two-tiered network planning, breaking away from the traditional cellular structure, to provide expected capacity increase for the future of wireless communications. In this novel paradigm, a second tier of densely deployed self-organizing small base stations (SBS) [1] is required to coexist with existing macro base station (MBS) infrastructure in a two-tiered network configuration.

Traditionally, coexistence in two-tiered networks can be achieved adopting three different approaches [2], [3]. *Complete separation*, where the MBS and SBSs operate on disjoint bands, avoiding cross-tier interference but decreasing the spectral efficiency. To enhance the spectral efficiency, *partial sharing* can be implemented. The two tiers share part of the total available band, and solutions for cross-tier interference management in the shared band need to be devised. The most attractive solution to maximize the spectral efficiency is represented by *complete sharing*, where the MBS and SBSs share the same band. Nevertheless, despite its notable features, this approach can easily bring unbearable amount of cross-tier interference from the SBSs to the MBS. Therefore, interference management techniques play a crucial role in such an approach and are fundamental for the coexistence of the two network tiers.

Solutions such as Interference Alignment [4] can be adopted to conceal the cross-tier interference at the receiver in a subset of the received signal space, but channel state information (CSI) and multiple dimensions at the transmitter and receiver are required. Joint beamforming [5] relies on CSI only at the transmitter, but can suffer from large power penalties depending on the number of involved MBSs/SBSs and the condition number of the resulting channel matrices. For non cooperative scenarios, cross-tier interference can then be managed through dynamic spectrum access (DSA). In this framework, SBSs can adopt strategies such as opportunistic interference alignment [6], spectrum shaping [7], cooperative frequency reuse [8], depending on the nature of the available left-over resources by the legacy tier.

In this contribution, we focus on the *complete sharing* approach and we propose a novel cognitive overlay [9] DSA technique for the SBSs, called multi-user VFDM (MU-VFDM). We aim at providing results for the upcoming network paradigms, thus we specifically target our efforts on the downlink of a future Long Term Evolution (LTE) [10] macro-cell, where an Orthogonal Frequency Division Multiple Access (OFDMA) MBS obliviously coexists with an

overlay cognitive SBS based network. MU-VFDM consists of cascaded linear precoder made up by an inner component designed to null the interference from the SBSs to the primary system, and an outer component to manage the interference in the second tier, modeled as a coordinated network Multiple Input Multiple Output (MIMO) system with infinite backhaul capacity. Therefore, both components of the precoder have beamforming tasks, whereas in standard two-steps signal processing at the transmitter the outer component typically has power loading purposes [11]. Remarkably, the availability of a perfect CSI at the transmitter is the only requirement to implement MU-VFDM, in contrast with the aforementioned state-of-the-art techniques that additionally need available left-over time, space or frequency resources. We show that, regardless of the considered number of SBSs, consistent sum-rate enhancements can be achieved w.r.t. to the legacy *complete separation* approach, for medium and high signal to noise ratio (SNR). Furthermore, the impact of imperfect CSI at the transmitter is evaluated providing important design insights.

This paper is organized as follows. In Sec. II, we introduce the general MBS/SBS model assumed throughout this paper. Then, we derive the precoders and briefly discuss their performance in Sec. III. In Sec. IV, we present some numerical results for our MBS/SBSs study case. Finally, conclusions and future research directions are discussed in Sec. V.

In this work, we adopt the mathematical notation as described in the following. A lower case italic symbol (e.g. $b$) denotes a scalar value, a lower case bold symbol (e.g. $\mathbf{b}$) denotes a vector, an upper case bold symbol (e.g. $\mathbf{B}$) denotes a matrix. $[\mathbf{B}]_{m,n}$ denotes a matrix element at the $m^{\text{th}}$ row and the $n^{\text{th}}$ column. An $\mathbf{I}_N$ denotes the identity matrix of size N. The transpose conjugate operator on a matrix is denoted by the H superscript (e.g. $\mathbf{B}^{\text{H}}$), the transpose operator is denoted by the T (e.g. $\mathbf{B}^{\text{T}}$) and the Moore-Penrose pseudoinverse matrix is denoted by $\dagger$ (e.g. $\mathbf{B}^{\dagger}$). The operator $\mathbf{A} \otimes \mathbf{B}$ is used to represent the Kronecker product, while $\mathbf{A} \circ \mathbf{B}$ is used for the Schur product. The special matrix $\mathbf{0}_{N,M}$ denotes the zero matrix of dimension $N \times M$. The symbol $[\cdot]_K$ denotes the modulo$-K$ operator, $\ker[\mathbf{A}]$ denotes the kernel of the matrix $\mathbf{A}$ and $\text{tr}(\mathbf{A})$ its trace. All vectors are columns, unless otherwise stated.

## II. System Model

Consider the downlink scenario in Fig. 1, where all communications are assumed to be in Time Division Duplex (TDD) mode. An MBS and $K$ SBSs, transmitting over the same frequency

band, are deployed in a given area.

The MBS serves $M$ single-antenna user equipments (MUEs). Cooperation between the SBSs is considered, yielding a full network MIMO transmission system model [12]. For simplicity, and without loss of generality, we assume that each SBS serves one single-antenna small-cell user equipment (SUE). Concerning the notation, subscript "m" refers to the MBS, while "s" refers to the SBSs, i.e., $h_{\text{sm}}^{(i,j)}$ (or $\mathbf{H}_{\text{sm}}^{(i,j)}$) represents a link from SBS $i$ to MUE $j$. Conversely, $\mathbf{s}^{[i]}$ (or $\mathbf{H}_{\text{sm}}^{([i],j)}$) denotes a vector/matrix related to the transmission from any SBS *except* $i$. All channel vectors $\mathbf{h}_{\text{ab}}^{(\cdot,\cdot)} \in \mathcal{CN}(0, \mathbf{I}_{L+1}/(L+1))$ represent the impulse response of independent and identically distributed (i.i.d.) frequency-selective Rayleigh fading channels composed of $L+1$ paths.

The MBS adopts an $M$-user OFDMA based transmission of block size $N+L$ and a cyclic prefix of size $L$. For simplicity, a uniform resource allocation of $N/M$ subcarriers per MUE is adopted, $\mathcal{N}_j$ being the set of subcarrier indexes assigned to MUE $j$ with $\bigcup_{j=1}^{M} \mathcal{N}_j = \{1, \ldots, N\}$ and $\bigcap_{j=1}^{M} \mathcal{N}_j = \emptyset$. As a consequence, each MUE selects its own set of subcarriers by means of a mask receiver filter $\mathbf{B}_j$, such that $\text{tr}(\mathbf{B}_j) = N/M$ and $\sum_{j=0}^{M} \mathbf{B}_j = \mathbf{I}_N$, with $[\mathbf{B}_j]_{(n,n)} = 1$ when the subcarrier $n$ is allocated to MUE $j$ and zero otherwise. Let $\mathbf{F} \in \mathcal{C}^{N \times N}$ be a unitary DFT matrix with $[\mathbf{F}]_{(k+1,l+1)} = \frac{1}{\sqrt{N}} e^{-i2\pi \frac{kl}{N}}$ for $k, l = \{0, \ldots, N-1\}$ and $\mathbf{A}$ a $(N+L) \times N$ cyclic prefix insertion matrix given by

$$\mathbf{A} = \left[ \begin{array}{c|c} \mathbf{0_{L,N-L}} & \mathbf{I}_L \\ \hline & \mathbf{I}_N \end{array} \right].$$

The channel matrix representing the link from the MBS to the $j^{th}$ MUE, after the cyclic prefix removal operation, is defined as $\mathcal{T}(\mathbf{h}_{\text{mm}}^{(1,j)}) \in \mathcal{C}^{N \times (N+L)}$ and constructed from the $\mathbf{h}_{\text{mm}}^{(\cdot,\cdot)}$ channel coefficients. In particular, the resulting Toeplitz matrix structure is given by

$$\mathcal{T}(\mathbf{h}_{\text{ab}}^{(\cdot,\cdot)}) = \begin{bmatrix} h_{\text{ab}}^{(\cdot,\cdot)}(L) & \cdots & h_{\text{ab}}^{(\cdot,\cdot)}(0) & 0 & \cdots & 0 \\ 0 & \ddots & & \ddots & \ddots & \vdots \\ \vdots & \ddots & \ddots & & \ddots & 0 \\ 0 & \cdots & 0 & h_{\text{ab}}^{(\cdot,\cdot)}(L) & \cdots & h_{\text{ab}}^{(\cdot,\cdot)}(0) \end{bmatrix}.$$

By summing up all the contributions of the MUEs, the equivalent channel matrix of the MBS is

$$\mathbf{H}_{\text{mm}} = \sum_{j=1}^{M} \mathbf{B}_j \mathbf{F} \mathcal{T}(\mathbf{h}_{\text{mm}}^{(1,j)}) \mathbf{A} \mathbf{F}^{-1}. \tag{1}$$

The overall interference channel from the SBSs to the MUEs is defined similarly to what is done for $\mathbf{H}_{\text{mm}}$. The equivalent channel for each of the SBSs is constructed as

$$\mathbf{H}_{\text{sm}} = \left[ \mathbf{H}_{\text{sm}}^{(1,\cdot)}, \ldots, \mathbf{H}_{\text{sm}}^{(K,\cdot)} \right], \tag{2}$$

thus the overall equivalent representation for each SBS is

$$\mathbf{H}_{\text{sm}}^{(i,\cdot)} = \sum_{j=1}^{M} \mathbf{B}_j \mathbf{F} \mathcal{T}(\mathbf{h}_{\text{sm}}^{(i,j)}). \tag{3}$$

Concerning the second tier, the SBSs adopt a block-transmission scheme that will be detailed in Sec. III-A. SUEs are not different from MUEs with respect to their reception chains, being distinguished merely by their association point (MBS or SBS). Therefore, like the MUEs, the SUEs discard the leading $L$ symbols and perform discrete Fourier transform (DFT) at the reception. Let $\mathbf{H}_{\text{ss}}^{(i,j)} = \mathcal{T}(\mathbf{h}_{\text{ss}}^{(i,j)}) \in \mathcal{C}^{N \times (N+L)}$ be the Toeplitz matrix representing the channel from the SBS $i$ to the SUE $j$. Then, by defining

$$\widetilde{\mathbf{H}}_{\text{ss}} = \begin{bmatrix} \mathbf{H}_{\text{ss}}^{(1,1)} & \cdots & \mathbf{H}_{\text{ss}}^{(1,K)} \\ \mathbf{H}_{\text{ss}}^{(2,1)} & \cdots & \mathbf{H}_{\text{ss}}^{(2,K)} \\ \vdots & \ddots & \vdots \\ \mathbf{H}_{\text{ss}}^{(K,1)} & \cdots & \mathbf{H}_{\text{ss}}^{(K,K)} \end{bmatrix}, \tag{4}$$

we can write the overall equivalent channel as

$$\mathbf{H}_{\text{ss}} = (\mathbf{I}_K \otimes \mathbf{F}) \widetilde{\mathbf{H}}_{\text{ss}}. \tag{5}$$

We can follow the same approach to model the interfering link from the MBS to the SUEs. By aggregating all the channel matrices, we define

$$\widetilde{\mathbf{H}}_{\text{ms}} = \begin{bmatrix} \mathbf{H}_{\text{ms}}^{(1,1)} \\ \mathbf{H}_{\text{ms}}^{(1,2)} \\ \vdots \\ \mathbf{H}_{\text{ms}}^{(1,K)} \end{bmatrix}, \tag{6}$$

where $\mathbf{H}_{\text{ms}}^{(1,j)} = \mathcal{T}(\mathbf{h}_{\text{ms}}^{(1,j)})\mathbf{A}\mathbf{F}^{-1} \in \mathcal{C}^{N\times N}, j \in [1, K]$. Consequently, the overall equivalent channel reads

$$\mathbf{H}_{\text{ms}} = (\mathbf{I}_K \otimes \mathbf{F})\widetilde{\mathbf{H}}_{\text{ms}}. \tag{7}$$

Let $\mathbf{y}_{\text{m}}^{(j)}, \mathbf{y}_{\text{s}}^{(j)}$ be the received $N$-sized vector at the j$^{th}$ MUE/SUE, respectively. As a consequence, $\mathbf{y}_{\text{m}} = \sum_{j=1}^{M} \mathbf{y}_{\text{m}}^{(j)}$ is the overall received vector at the MUEs of size $N$, and $\mathbf{y}_{\text{s}} \triangleq [\mathbf{y}_{\text{s}}^{(1)\text{T}}, \ldots, \mathbf{y}_{\text{s}}^{(K)\text{T}}]^{\text{T}}$ is the overall received vector at the SUEs of size $N \times K$, obtained by aggregating each SUE's received component. Furthermore, we define $\mathbf{s}_{\text{m}}$ as the MBS input vector of size $N$, composed of $M$ individual zero mean, unit norm symbol vectors $\mathbf{s}_{\text{m}}^{(j)},\ j \in [1, M]$, and $\mathbf{x}_{\text{s}} \triangleq [\mathbf{x}_{\text{s}}^{(1)\text{T}}, \ldots, \mathbf{x}_{\text{s}}^{(M)\text{T}}]^{\text{T}}$ as the overall SBS transmit vector, detailed later for clarity. The resulting signal model is then

$$\begin{aligned} \mathbf{y}_{\text{m}} &= \mathbf{H}_{\text{mm}}\mathbf{s}_{\text{m}} + \mathbf{H}_{\text{sm}}\mathbf{x}_{\text{s}} + \mathbf{F}\mathbf{n}_{\text{m}} \\ \mathbf{y}_{\text{s}} &= \mathbf{H}_{\text{ss}}\mathbf{x}_{\text{s}} + \mathbf{H}_{\text{ms}}\mathbf{s}_{\text{m}} + (\mathbf{I}_K \otimes \mathbf{F})\mathbf{n}_{\text{s}}. \end{aligned} \tag{8}$$

Note that, in (8), $\mathbf{n}_{\text{m}} \sim \mathcal{CN}(0, \sigma^2\mathbf{I}_N)$ and $\mathbf{n}_{\text{s}} = [\mathbf{n}_{\text{s}}^{(1)\text{T}}, \ldots, \mathbf{n}_{\text{s}}^{(K)\text{T}}]^{\text{T}} \sim \mathcal{CN}(0, \sigma^2\mathbf{I}_{KN})$ are additive white gaussian noise (AWGN) vectors.

## III. Precoder Design

According to the cognitive overlay paradigm [13], the secondary system must protect the primary network from the interference caused by the opportunistic transmission. By looking at (8), we see that this implies

$$\mathbf{H}_{\text{sm}}\mathbf{x}_{\text{s}} = \mathbf{0}. \tag{9}$$

The transmitted message by the MBS to the MUEs is not known in the secondary system, thus dirty paper coding (DPC) [14] based algorithms to cancel the cross-tier interference can not be implemented. No information about time, space or frequency left-over resources by the primary system is available at the SBSs and, in particular, each MUE has only one available spatial dimension. Therefore, traditional techniques to design an interference-free transmission [4]-[8] can not be implemented in the considered scenario.

One of the features of cognitive radio networks [9], is the flexibility of the adopted physical and network layer strategies, such that the secondary system can easily respond to any change in the primary system. As a consequence, in this context, implementable DSA techniques through conventional digital signal processing at the transmitter are attractive solutions. To this purpose,

we focus our attention on linear approaches to cancel the interference from the SBSs to the MUEs.

Let $\mathbf{s}_\mathrm{s}$ be the aggregated SBSs' input vector, such that the SBSs' aggregated transmit vector $\mathbf{x}_\mathrm{s} = \mathbf{E}\mathbf{s}_\mathrm{s}$ becomes its linearly precoded version through $\mathbf{E}$. Then (9) can be rewritten as

$$\mathbf{H}_\mathrm{sm}\mathbf{E} = \mathbf{0}, \tag{10}$$

with $\mathbf{E}$ and $\mathbf{s}_\mathrm{s}$ detailed later for clarity. If we assume that each SBS may independently precode its input vector to cancel the interference towards the MUEs, resulting both in a simpler architecture and in a lower backhaul signaling, we can express $\mathbf{E}$ as the direct sum [15] of $K$ precoders

$$\mathbf{E} = \bigoplus_{i=1}^{K} \mathbf{E}_i, \tag{11}$$

where $\mathbf{E}_i$ is the precoder at the $i^{th}$ SBS. It is straightforward to see when the following holds

$$\mathbf{H}_\mathrm{sm}^{(i,\cdot)}\mathbf{E}_i = \mathbf{0}, \quad \forall i \in [1, K], \tag{12}$$

(10) is always satisfied, if perfect CSI at the transmitter (CSIT) is available at the SBSs. As a consequence, we can focus on the $i^{th}$ SBS to devise $\mathbf{E}_i$ and then apply (11) to find the desired overall precoder. We remark that, in this section, we assume perfect CSIT related to the interfering links from the SBSs towards the MUEs. In the second part of the work, the impact of an imperfect CSIT will be analyzed.

### *A. Single SBS/SUE Precoder Design*

Consider the fictious scenario illustrated in Fig. 2 given by the $i^{th}$ SBS and its SUE $j$, that is, $K = 1$. In [16], we proposed a linear precoder to solve the interference cancelation problem in a similar scenario, where the SBS deals with a primary OFDM downlink. A roots-based algorithm called VFDM was derived, starting from the polynomial representation of the interference channel. Unfortunately, unlike in [16], the considered SBS deals with a multi-user OFDMA downlink. Due to the multiple interfering links from the SBS to the MUEs, no polynomial representation of the equivalent channel is possible, and the Vandermonde-subspace based result is not directly applicable to our case. Therefore, in the following, we extend the applicability of the aforementioned technique to the current scenario.

By looking at (12), we note that, if this precoder exists, then it must lie within the kernel of $\mathbf{H}_\mathrm{sm}^{(i,\cdot)}$. Now let $\mathbf{H}_\mathrm{sm}^{(i,\cdot)} = \mathbf{L}\mathbf{Q}$ be the LQ decomposition of the equivalent channel matrix

representing the interfering link between the $i^{th}$ SBS and the MUEs, where $\mathbf{L} \in \mathcal{C}^{N\times(N+L)}$ is a lower triangular matrix and $\mathbf{Q} \in \mathcal{C}^{(N+L)\times(N+L)}$ is a unitary matrix given by

$$\mathbf{Q} \triangleq [\ \mathbf{q}_1 \mid \mathbf{q}_2 \mid \cdots \mid \mathbf{q}_{N+L}\ ]. \tag{13}$$

By construction, $\mathrm{rank}\,(\mathbf{H}_{\text{sm}}^{(i,\cdot)}) = N$, hence we know that the last $L$ orthonormal columns of $\mathbf{Q}^{\text{H}}$ lie within $\ker\,(\mathbf{H}_{\text{sm}}^{(i,\cdot)})$. Thereupon, if we define

$$\mathbf{E}_i \triangleq \left[\ \mathbf{q}_{N+1} \mid \cdots \mid \mathbf{q}_{(N+L)-1} \mid \mathbf{q}_{N+L}\ \right], \tag{14}$$

we have an orthogonal precoder that fulfills (12). We first focus on the MBS. If we plug $\mathbf{E}_i$ in (8), we obtain

$$\mathbf{y}_{\text{m}} = \mathbf{H}_{\text{mm}}\mathbf{s}_{\text{m}} + \nu_{\text{m}}, \tag{15}$$

where $\nu_{\text{m}} \in \mathcal{CN}(0, \sigma_n^2\mathbf{I}_N)$ is the DFT of the AWGN vector $\mathbf{n}_{\text{m}}$, having the same size and statistic.

Concerning the secondary link, we can write $\mathbf{y}_{\text{s}}^{(j)}$ as

$$\mathbf{y}_{\text{s}}^{(j)} = \mathbf{H}_{\text{ss}}^{(i,j)}\mathbf{E}_i\mathbf{s}_{\text{s}}^{(i)} + \mathbf{H}_{\text{ms}}^{(1,j)}\mathbf{s}_{\text{m}} + \nu_{\text{s}}^{(j)}, \tag{16}$$

where $\mathbf{E}_i \in \mathcal{C}^{(N+L)\times L}$ is the desired linear precoder, $\mathbf{H}_{\text{ss}}^{(i,j)} = \mathbf{F}\mathcal{T}(\mathbf{h}_{\text{ss}}^{(i,j)}) \in \mathcal{C}^{N\times(N+L)}$ is the matrix representing the link from the considered SBS to its SUE, $\mathbf{s}_{\text{s}}^{(i)}$ is the individual zero mean, unit norm $L$-sized $i^{th}$ SBS' input symbol vector and $\nu_{\text{s}}^{(j)} \in \mathcal{CN}(0, \sigma_n^2\mathbf{I}_N)$ is the DFT of $\mathbf{n}_{\text{s}}^{(j)}$. By looking at (16), it is important to point out that each SBS has an implicit upper bound on the number of input symbols that can be precoded, i.e. $L$, to guarantee a not harmful transmission w.r.t. the MUEs. This, together with the perfect CSIT assumption, is the cost of the interference cancelation constraint induced by the overlay cognitive approach. Nonetheless, we note that, unlike other interference management schemes that exploit the spatial degrees of freedom by the use of multiple antennas, i.e. zero forcing (ZF) or IA, the proposed technique requires only one antenna per SBS. In fact, the interference towards the primary system is canceled by adopting a precoder $\mathbf{E}_i$ that opportunistically exploits the redundancy introduced by the MBS to combat inter symbol (ISI) and inter block interference (IBI), e.g. the cyclic prefix. In the following, we start from these findings to analyze the multi SBS/SUE scenario described in Sec. II.

### B. Multi SBS/SUE VFDM Precoder Design

As seen in Sec. III-A, the SBSs disjointly design the precoders $\mathbf{E}_i \ \ \forall i \in [1, K]$, such that the overall precoder $\mathbf{E}$ as shown in (11) successfully satisfies (9). Taking $\mathbf{E}$ into consideration, we can rewrite the signal model in (8) as

$$\begin{aligned} \mathbf{y}_{\mathrm{m}} &= \mathbf{H}_{\mathrm{mm}}\mathbf{s}_{\mathrm{m}} + \mathbf{F}\mathbf{n}_{\mathrm{m}} \\ \mathbf{y}_{\mathrm{s}} &= \mathbf{H}_{\mathrm{ss}}\mathbf{E}\mathbf{s}_{\mathrm{s}} + \mathbf{H}_{\mathrm{ms}}\mathbf{s}_{\mathrm{m}} + \nu_{\mathrm{s}}, \end{aligned} \tag{17}$$

where $\mathbf{E} \in \mathcal{C}^{K(N+L)\times KL}$ is the overall precoder and $\mathbf{s}_{\mathrm{s}}$ is the $KL$-sized aggregated zero mean, unit norm SBS transmitted symbol vector. At this stage, it is also clear by looking at (8), that $\mathbf{x}_{\mathrm{s}}$, overall transmit vector at the SBSs, whose characteristics were previously omitted,is composed of $K$ $(N+L)$-sized transmit vector $\mathbf{x}_{\mathrm{s}}^{(i)} = \mathbf{E}_i\mathbf{s}_{\mathrm{s}}^{(i)}$, thus can only have size can only have size $M(N+L)$.

We focus on the second tier and, for clarity, we simplify the notation by introducing

$$\overline{\mathbf{H}}_{\mathrm{ss}} = \mathbf{H}_{\mathrm{ss}}\mathbf{E}. \tag{18}$$

The structure of the received signal is the same for any SUE, hence we can rewrite (16) for MU-VFDM as

$$\mathbf{y}_{\mathrm{s}}^{(j)} = \overline{\mathbf{H}}_{\mathrm{ss}}^{(i,j)}\mathbf{s}_{\mathrm{s}}^{(i)} + \overline{\mathbf{H}}_{\mathrm{ss}}^{([i],j)}\mathbf{s}_{\mathrm{s}}^{[i]} + \mathbf{H}_{\mathrm{ms}}^{(1,j)}\mathbf{s}_{\mathrm{m}} + \nu_{\mathrm{s}}^{(j)}, \tag{19}$$

in which, we identify a useful component, two interfering terms and the thermal noise. In (19), $\overline{\mathbf{H}}_{\mathrm{ss}}^{([i],j)}\mathbf{s}_{\mathrm{s}}^{[i]}$ represents the multiuser interference experienced by each SUE. Therefore, the performance of the SBSs hinges on $K$ and can be strongly interference limited. Note that, the absence of cooperation between the two tiers implies that the MBS' interference on the SUEs is always present. Consequently, in this scenario each SUE deals with a stronger interference if compared to the single SBS case in Sec. III-A. To address this issue, we assume that the SBSs may cooperate, realizing a coordinated network MIMO system, to mitigate the multi-user interference. The SBSs can be therefore modeled as a MIMO-BC, whose capacity is given by DPC [17] whose its implementation is, in the best case, very challenging. Because of its complexity, many suboptimal but linear strategies have been introduced lately. In the following section we discuss the advantages and disadvantages of several of these linear transmit schemes when applied to our scenario. We aim at identifying a suitable linear technique to exploit the

cooperation between the SBSs, achieving the highest sum-rate values, when compared to the maximum achievable sum-rate using DPC.

### *C. Practical Transmit Schemes*

In (17), we focus on the SBSs' transmission by isolating the term $\overline{\mathbf{H}}_{\text{ss}}$ of dimension $KN \times KL$, as defined in (18). Note that, in any block transmission system, the transmitter tries to minimize the added redundancy $L$ to the block of $N$ useful symbol, for matters of efficiency. In particular, it is always verified that $\frac{L}{N} < 1$. Therefore, in MU-VFDM, each transmitter faces a dimensionality constraint to cancel the interference towards the MBS. This implies that a direct application of techniques such as zero force beamforming (ZFBF) [18] or block diagonalization (BD) [19] is not possible, since both require that the transmit dimensions be bigger or equal than the receiver dimensions. Regularized inverse beamforming (RIBF) [20] is applicable, but it achieves poor performance at high SNR, due to the aforementioned dimensionality issue ($N > L$ received symbols) that yields a very poor condition number to the equivalent channel representation built upon Toeplitz matrices. Matched Filter (MF) precoding [21] performs similarly, being largely suboptimal at high SNR. It is known from [22], and for the multiple beams case from [23], that opportunistic random beamforming (ORBF) based techniques are able to yield the optimal capacity scaling of $M \log \log K$ in dense networks with a large number of receivers. Unfortunately, in our scenario the ratio $\frac{N}{L}$ is such that we can not achieve good performance using these techniques. In general, most of the results in the literature regarding linear precoding techniques under given optimization criteria assume only one antenna/symbol at the receiver. For this reason, a direct extension of these techniques is not possible.

In general, algorithms like successive MMSE precoding (SMMSE) [24] and iterative regularized block diagonalization (IRBD) [25] deal with multiple symbols/antennas at each receiver. The higher diversity gain they provide is due to the suppression of the interference only between the symbols received by two different receivers. These algorithms perform better than other techniques that rely on the single antenna/symbol assumption, but on the other hand they require a joint receiver decoding with a consequent increase in the complexity of the receivers' architecture.

Simpler solutions, implemented to deal with an arbitrary number of dimensions at each receiver, are user/antenna selection based algorithms. It is known that by scheduling only a subset of antennas or eigenmodes [19] to be served using a classical ZFBF, the achievable sum-

rate is asymptotically optimal [26]. In spite of this, the condition for the asymptotic optimality is never met in a MU-VFDM system, thus neither an exhaustive search of the optimal subset nor a faster and suboptimal greedy selection algorithm [27] can achieve good results.

Looking at the schemes presented thus far, we note that the inherent dimensionality constraint limits the performance of the second tier, in terms of both achievable sum-rate and complexity of the SBSs/SUEs. Starting from this consideration, we propose a low complexity solution to overcome the dimensionality constraint and manage multi-user interference in the following section.

### *D. RIBF Flexible Network Solution*

As stated previously, a strategy to overcome the dimensionality constraint inherent to MU-VFDM needs to be found, without reducing the number of considered dimensions at the receivers. We introduce the *load rate* $\beta$ as the ratio between the number of dimensions at the transmitter and the ones at the receiver

$$\beta = \frac{\psi_{tx}}{\psi_{rx}}. \tag{20}$$

In our specific case, we let $\psi_{tx} = \gamma_{tx} L$ and $\psi_{rx} = \gamma_{rx} N$, where $L$ and $N$ are fixed due to the OFDMA symbol structure. $\gamma_{tx}$ and $\gamma_{rx}$ are two parameters related respectively to the transmitter and receiver, depending on the chosen SBS layout or SBS/SUE architecture, hence, to the dimensionality of the system. As a consequence, by changing the number of dimensions at the SBSs/SUEs, we effectively change the number of available channels for the transmission. For instance, when $\gamma_{tx} = 1$ and $\gamma_{rx} \to \infty$, we consider a greater number of SUEs (or SUEs' antennas) from which the best ones to serve are selected, and this represents the condition under which ORBF is optimal. Conversely, if $\gamma_{rx}$ is kept constant ($\gamma_{rx} = 1$ for simplicity) and we let $\gamma_{tx}$ increase, the SBSs can exploit the available dimensions per SUE to achieve a higher diversity, thanks to the greater number of considered channels. Another interesting configuration is given by $\gamma_{tx} = N$ and $\gamma_{rx} = L$, that is a network where the number of dimensions at SBS/SUE coincides, i.e., RIBF becomes efficient in terms of degrees of freedom exploitation.

In this way, $L$ and $N$ fixed, the system designer can tune $\gamma_{tx}$ and $\gamma_{rx}$ to capitalize on the flexibility of the model through the addition of more antennas at each SBS/SUE, or alternatively by increasing the SBS' density. In our scenario, to overcome the dimensionality constraint, we

need to add more dimensions at the transmitter until the following holds

$$\gamma_{tx} L \geq \gamma_{rx} N. \tag{21}$$

Then, without loss of generality, let $\gamma_{rx} = 1$ and $\gamma_{tx}$ increase. In particular, we note that this preserves the legacy number of antennas per SUE, i.e., 1, and their disjoint decoding strategy. Due to the large number of SBSs (or antennas per SBS), we consider a uniform power allocation strategy to reduce the computational burden for the SBSs. We remark that, thanks to the $\gamma_{rx}$ and $\gamma_{tx}$ tuning, the second tier is characterized by a greater number of channels. As a consequence, in the new setup, $\mathbf{s}_{\mathrm{s}}$ is a $\gamma_{tx}KL-$sized vector, $\mathbf{E} \in \mathcal{C}^{\gamma_{tx}K(N+L)\times\gamma_{tx}KL}$ and $\overline{\mathbf{H}}_{\mathrm{ss}} \in \mathcal{C}^{KN\times\gamma_{tx}KL}$. At this stage, we focus on the choice of an appropriate linear transmit scheme. As noted in Sec.III-C, the difference in terms of sum-rate between the considered techniques is reasonably small, especially if we restrict our attention to low complexity one step solutions. We focus on the three main techniques based on a one step linear processing at the transmitter: ZF, MF and RIBF. It is known [28] that a MF approach is optimal for low SNR, while ZF is asymptotically optimal at high SNR. RIBF exhibits interesting features for low SNR, providing comparable performance to MF and, on the other hand, behaves asymptotically as ZF for high SNR. Consequently, RIBF is the natural choice if we want to guarantee good performance at any SNR and we let

$$\mathbf{\Phi} = \overline{\mathbf{H}}_{\mathrm{ss}}^{\mathrm{H}}(\frac{\sigma_n^2}{P_s}\mathbf{I}_{KN} + \overline{\mathbf{H}}_{\mathrm{ss}}\overline{\mathbf{H}}_{\mathrm{ss}}^{\mathrm{H}})^{-1} \tag{22}$$

be the joint RIBF precoder, $\mathbf{\Phi} \in \mathcal{C}^{\gamma_{tx}KL\times KN}$. Then, if we let $\mathbf{u}_{\mathrm{s}} \in \mathcal{C}^{KN\times 1}$ be a new aggregated SBSs' input symbol vector, such that $\mathbf{s}_{\mathrm{s}} = \mathbf{\Phi}\mathbf{u}_{\mathrm{s}}$ we can rewrite the signal model in (17) as follows

$$\begin{aligned} \mathbf{y}_{\mathrm{m}} &= \mathbf{H}_{\mathrm{mm}}\mathbf{s}_{\mathrm{m}} + \mathbf{F}\mathbf{n}_{\mathrm{m}} \\ \mathbf{y}_{\mathrm{s}} &= \mathbf{H}_{\mathrm{ss}}\mathbf{W}\mathbf{u}_{\mathrm{s}} + \mathbf{H}_{\mathrm{ms}}\mathbf{x}_{\mathrm{m}} + \nu_{\mathrm{s}}, \end{aligned} \tag{23}$$

where

$$\mathbf{W} = \frac{\mathbf{E}\mathbf{\Phi}}{\sqrt{\mathrm{tr}(\mathbf{E}\mathbf{\Phi}\mathbf{\Phi}^{\mathrm{H}}\mathbf{E}^{\mathrm{H}})}} \in \mathcal{C}^{\gamma_{tx}K(N+L)\times KN} \tag{24}$$

is the overall normalized MU-VFDM precoder, such that $\mathrm{tr}(\mathbf{W}^{\mathrm{H}}\mathbf{W}) = 1$. Once the condition in (21) is fulfilled, a two-stage signal processing at the SBSs can be performed with a cascade of two precoders. The SBSs cooperate to perform an outer precoding $\mathbf{\Phi}$ to implement RIBF towards the SUEs. Conversely, the inner precoder $\mathbf{E}$ is created with no cooperation between

SBSs, as seen in Sec. III-A, to decrease the required signaling burden. This comes in contrast to what is typically done in a two stage signal processing at the transmitter (e.g. [11]), where the outer stage has solely power optimization and allocation purposes. Furthermore, we emphasize that, the cascaded precoder structure is intrinsically different from that of our previous works in [16], even for the $K, M = 1$ case. In fact, the use of an outer linear precoding scheme, while preserving the interference cancelation condition towards the MBS system, substantially changes the dimensionality of the system.

## IV. Numerical Analysis

In this section, we present a numerical performance analysis of the proposed technique. Please note that, according to Sec. II and III, the matrices $\mathbf{H}_{\text{sm}}$ and $\mathbf{E}$ are not composed of i.i.d. random entries, but are strongly structured. No closed form of the eigenvalue/eigenvector distribution is available, and a purely theoretical performance analysis can not be carried out. Consequently, we proceed by means of Monte Carlo based simulations of the considered downlink scenario, comprised of an OFDMA/LTE MBS in the macro cell with $M = 4$ MUEs, and an MU-VFDM based small cell system. For simplicity, we consider the least resource-demanding extended mode proposed by the standard [10], and characterized by $N = 128$ subcarriers, a cyclic prefix of length $L = 32$, for a total bandwidth of 1.92 MHz. Noise and channel vectors are generated as described in Sec. II. First we assume that a perfect CSI is available at the SBSs, afterwards we admit for the presence of noisy channel estimation yielding imperfect CSIT. Note that, if not stated otherwise in the text, we do not consider any interference from the MBS to the SUEs to isolate the effect of the MU-VFDM precoder on second tier's performance. In particular, this assumption is crucial to evaluate the effect of the imperfect channel estimation at the SBSs on the performance of the cascaded precoder designed in Sec. III.

### A. Multi-User VFDM

Consider a small cell system composed by $K = 3$ SBSs/SUEs. It is well known that the maximum ergodic sum-rate of a MIMO-BC, $C^{\text{SUM}}$, is achievable by DPC [17]. Now, let $\mathcal{B}$ be the considered bandwidth and $P_s = P_m$ be the power per transmit symbol at each SBS and at the MBS respectively. We can compute $C^{\text{SUM}}_{\text{DPC}}$ for uniform power allocation as follows [28]

$$C^{\text{SUM}}_{\text{DPC}} = \frac{\mathcal{B}}{N+L}\mathbb{E}\left[\log_2\left|\mathbf{I}_{KN} + \left(\frac{N+L}{\sigma^2 L\gamma_{tx}}\right) P_s \overline{\mathbf{H}}_{\text{ss}}\overline{\mathbf{H}}^H_{\text{ss}}\right|\right]. \tag{25}$$

In Fig. 3, the behavior of the upper bound $C_{\text{DPC}}^{\text{SUM}}$ is shown and compared to the achievable ergodic sum-rate $C^{\text{SUM}}$ for several linear precoding strategies, for SNR $\in [0, 35]$. In addition to the techniques described in Sec. III-C, we tested other solutions such as, the SVH algorithm [29] with 20 iterations, the ISSMSE (an iterative version of the SMMSE algorithm inspired by [25]) with 40 iterations and, finally, the semi-orthogonal user selection ZFBF (SUS-ZFBF) algorithm proposed in [26]. The behavior of the considered linear precoding schemes shows a big rate offset when compared to the upper bound represented by DPC, and this confirms what has been discussed in Sec. III-C.

To compute the sum-rate of the small cell system implementing RIBF, $C_{\text{RIBF}}^{\text{SUM}}$, we need to evaluate the signal to interference plus noise ratio (SINR) for any of the $KN$ received symbols at each SUE. Let $\mathbf{\Phi} = [\boldsymbol{\phi}^{(1)}, \ldots, \boldsymbol{\phi}^{(KN)}]$. Let $\overline{\mathbf{h}}_{\text{ss}}^{(j)} = [[\overline{\mathbf{H}}_{\text{ss}}]_{j1}, \ldots, [\overline{\mathbf{H}}_{\text{ss}}]_{j\gamma_{tx}KL}]^T$ denote the $j^{th}$ row of $\overline{\mathbf{H}}_{\text{ss}}$, then we can write

$$\text{SINR}_{(\text{s}),j} = \frac{|\overline{\mathbf{h}}_{\text{ss}}^{(j)} \boldsymbol{\phi}^{(j)}|^2}{\sum_{i \neq j}^{KN} |\overline{\mathbf{h}}_{\text{ss}}^{(j)} \boldsymbol{\phi}^{(i)}|^2 + \frac{\text{tr}(\mathbf{W}\mathbf{W}^{\text{H}})\sigma_n^2}{P_s K(N+L)}}, \quad \forall j \in [1, KN] \tag{26}$$

where we recall that the dimension of $\overline{\mathbf{H}}_{\text{ss}}$ depends strictly on the value assumed by $\beta$. Then, it is straightforward to see that for a $K-$SBS system the achievable sum-rate, when perfect CSIT is available, is given by

$$C_{\text{RIBF}}^{\text{SUM}} = \frac{\mathcal{B}}{N+L} \sum_{j=1}^{KN} \log_2(1 + \text{SINR}_{(\text{s}),j}). \tag{27}$$

In Fig. 4 we illustrate a comparison between $C_{\text{RIBF}}^{\text{SUM}}$ and $C_{\text{DPC}}^{\text{SUM}}$, for a load rate of $\beta = 3$, confirming that the proposed technique has comparable performance to state-of-the-art solutions. We remark that, the complexity of the linear precoding techniques outperforming RIBF in Fig. 3 prevents their implementability for $\beta > \frac{L}{N}$. This consideration further motivates the proposed solution for the multi-user VFDM dense network deployment. Due to the inherent simplicity of the proposed solution, the SBSs' performance can be made arbitrarily close to the upper bound, by increasing the number of dimensions at the transmit side.

Finally, in Fig. 5 we show how the sum-rate increases with the number of SBSs. Moreover, thanks to the precoder $\mathbf{E}$, the SBSs protect the MUEs from interference, effectively increasing the spectral efficiency and the capacity per area. Consequently, the coexistence in the two-tiered network can be effectively realized yielding significant gains.

*B. Imperfect CSIT*

In Sec. III, we showed that when a perfect CSIT is available at the SBSs, an interference nulling precoder $\mathbf{E}$ can be designed. However, in a realistic implementation, each transmitter in the system performs noisy channel estimations, yielding an imperfect CSIT. Therefore, in this section, we seek for a deeper understanding of the impact of the CSIT acquisition on the overall network performance. We recall that in Sec. II we assumed an infinite backhaul capacity. This allows us to target our efforts on the analysis of the effect of a noisy channel estimation onto the performance of the two-tiered network. The study of the achievable performance for a two-tiered network operating under limited backhaul capacity, and the impact of the quantization of the CSI, will be subject of a future work. The design of a suitable channel estimation procedure is out of the scope of this work as well, thus, for simplicity, we assume a classic training/transmission scheme as in [30].

Consider a block fading channel model where a channel estimation is valid throughout the duration of the coherence time $T$. The channel estimations are performed during a period $\tau \leq T$, hence the available time for transmission is upper bounded by $T - \tau$. During the training phase the devices broadcast orthonormal sequences of known pilot symbols of equal power. Each channel observation can be expressed as

$$\mathbf{r} = \sqrt{\rho\tau}\mathbf{h} + \mathbf{n},$$

where $\mathbf{h}$ is the channel vector, $\rho$ is the SNR at the receiver and $\mathbf{n} \sim \mathcal{CN}(0, \sigma_n^2 \mathbf{I}_{(L+1)})$ models the effects of the thermal noise at the devices' antennas. Each device computes the minimum mean-square error (MMSE) estimate of $\mathbf{h}$, by evaluating the observation $\mathbf{r}$. Then $\mathbf{h}$ is decomposed into two components, i.e., an estimate $\hat{\mathbf{h}}$ and an independent error $\tilde{\mathbf{h}}$, that is

$$\mathbf{h} = \hat{\mathbf{h}} + \tilde{\mathbf{h}}.$$

Without the perfect CSI assumption at the SBSs, the zero interference constraint in (9) can no longer be satisfied, thus the SBSs may generate interference towards the MUEs. If we denote the $j^{th}$ row of $\mathbf{H}_{\text{mm}}$ as $\mathbf{h}_{\text{mm}}^{(j)} = [[\mathbf{H}_{\text{mm}}]_{j1}, \ldots, [\mathbf{H}_{\text{mm}}]_{jN}]^T$, and the $j^{th}$ row of $\mathbf{H}_{\text{sm}}$ as $\mathbf{h}_{\text{sm}}^{(j)} = [\mathbf{H}_{\text{sm}}]_{j1}, \ldots, [\mathbf{H}_{\text{sm}}]_{j\gamma_{tx}KL}]^T$, then the SINR per received symbol at the MUEs reads

$$\text{SINR}_{(\text{m}),j} = \frac{P_m K |\mathbf{h}_{\mathbf{h}_{\text{mm}}}^{(j)}|^2}{\sum_{i=1}^{KN} |\mathbf{h}_{\text{sm}}^{(j)} \boldsymbol{\phi}^{(i)}|^2 + \sigma_n^2}, \forall j \in [1, N]. \tag{28}$$

For the SUEs, an imperfect CSI at the SBSs has an impact on the design of $\mathbf{W}$, worsening the SINR per received symbol, due to channel estimation effects and increased multi-user interference component. Thereupon, (26) does not hold for this case and each SUE experiences an effective SINR value [30] per received symbol as given by

$$\text{SINR}_{(\text{s}),j} = \frac{\left(\frac{|\overline{\mathbf{h}}_{\text{ss}}^{(j)}\boldsymbol{\phi}^{(j)}|^2}{\sum_{i\neq j}^{KN}|\overline{\mathbf{h}}_{\text{ss}}^{(j)}\boldsymbol{\phi}^{(i)}|^2+\frac{\mathbf{tr}(\mathbf{W}\mathbf{W}^{\text{H}})\sigma_n^2}{P_s K(N+L)}}\right)^2\tau}{1+(1+\tau)\frac{|\overline{\mathbf{h}}_{\text{ss}}^{(j)}\boldsymbol{\phi}^{(j)}|^2}{\sum_{i\neq j}^{KN}|\overline{\mathbf{h}}_{\text{ss}}^{(j)}\boldsymbol{\phi}^{(i)}|^2+\frac{\mathbf{tr}(\mathbf{W}\mathbf{W}^{\text{H}})\sigma_n^2}{P_s K(N+L)}}}, \forall j \in [1, KN], \tag{29}$$

where we assume that the same transmit power is used for training and data symbols. Then, the sum-rate of the MBS and SBSs respectively is

$$\begin{aligned} C_{\text{m}}^{\text{SUM, I}} &= \frac{T-\tau}{T(N+L)}\sum_{j=1}^{N}\log_2(1+\text{SINR}^{\text{eff}}(\text{m}),j) \\ C_{\text{s}}^{\text{SUM, I}} &= \frac{T-\tau}{T(N+L)}\sum_{j=1}^{KN}\log_2(1+\text{SINR}^{\text{eff}}(\text{s}),j). \end{aligned}$$

To reduce Monte Carlo simulation times, we consider $N = 24$ active subcarriers, cyclic prefix length of $L = 6$ and a load rate of $\beta = 1$. In Fig. 6, the ratio between the rate obtained with imperfect CSIT and the rate obtained with perfect CSIT is computed for the MBS system as different $\tau/T$ proportions are chosen for SNR $\in \{0, 10, 20\}$ dB. The optimal $\tau$ shows a dependency on the SNR and, in particular, an optimal value can be identified in the very low SNR regime, i.e., $\tau = 0.16T$. On the other hand, for medium and high SNRs the best performance is obtained for the minimum value given the considered parameters, i.e., $\tau = 0.08T$. We note that, the sum-rate scales linearly with the pre-log factor in this regime. Interestingly, the performance for different SNR values is very similar. Furthermore, by comparing the rate loss for SNR $\in \{10, 20\}$ dB we clearly see an almost constant behavior independent from the considered SNR.

In Fig. 7, the ratio between the rate obtained with imperfect CSIT and the rate obtained with perfect CSIT for the SBSs is computed for the same SNR range and $\beta$ value. Differently from what we have seen for the MBS, for the SBSs system a bigger training time results always in a power gain, thus optimal values for $\tau$ can be identified for any SNR regime. We note that, if compared to the loss experienced by the macro cell, a worse CSIT affects mainly the sum-rate of the small cells that can be penalized especially at very low SNR.

To conclude the analysis on the impact of the imperfect CSIT on the performance of the two-tiered network, we test how MU-VFDM can perform consistently as the transmit dimensions increase. We assume a constant SNR$= 10$ dB. To increase the transmit dimensions in the second tier we can either install more antenna on each SBS, i.e., $\beta$ increases, or deploy more SBSs, i.e., $K$ increases. Therefore, we let the load rate $\beta \in \{1, 1.5, 2\}$ in Fig. 8, and the number of SBSs $K \in \{2, 3, 4\}$ in Fig. 9. By comparing the two cases, MU-VFDM shows a remarkable robustness and effectiveness regardless of the adopted approach. Moreover, in both cases, the difference in the performance of the MBS, as the considered parameter changes, is negligible and the best results are obtained for the minimum value of $\tau$. For the SBSs, on the contrary, we can see that increasing the number of antennas is more effective than deploying an extra SBS. The ratio between the rate obtained with imperfect CSIT and the rate obtained with perfect CSIT for the SBSs is better for the first approach. The difference in the performance, as the considered parameter changes, reinforces this results even further, showing a larger gap for the second approach.

### *C. Comparison with existing solutions*

In this section, we evaluate the performance of the proposed scheme by comparing MU-VFDM to state-of-the-art techniques that allow the deployment of a two-tiered network [2]: 1) *Complete sharing*, 2) *partial sharing*, 3) *complete separation*. MU-VFDM allows the coexistence of SBSs and MBS inside the same area, nulling the interference from the former to the latter, adopting a complete sharing approach. Among the aforementioned bandwidth management schemes, only the complete separation approach guarantees zero interference from the SBSs to the MBS. Therefore, for a fair comparison, we focus on this approach and divide the available bandwidth in two portions assigned exclusively to the MBS and the SBSs. Considering the values introduced previously, i.e., $N = 24$ and $L = 6$, this implies that both the MU-VFDM and the complete separation based system transmit over a bandwidth $\mathcal{B} = 0.48$ MHz. As seen in Sec. III-A, by implementing MU-VFDM, each SBS can transmit up to $L$ input symbols from each SBS' antenna. On the other hand, the MBS transmits $N$ input symbols, i.e., the number of considered subcarriers. Consequently, in the complete separation approach, we assign a bandwidth $\mathcal{B}_s = \frac{\mathcal{B}L}{N}$ to the SBSs and $\mathcal{B}_m = \mathcal{B} - \mathcal{B}_s$ to the MBS. By means of this division, we ensure that each SBS' antenna is transmitting the same number of symbols as in MU-VFDM. Moreover, in order to

exploit all the available transmit dimensions, we assume that the SBSs perform a network MIMO-OFDMA transmission towards the SUEs, adopting a ZF precoding such that no linear processing at the SUEs is required, as in MU-VFDM. Note that, a legacy OFDMA transmission is performed by the MBS as described previously. As a last remark, differently from what we have assumed so far, we assume that in MU-VFDM the SUEs suffer from full interference from the MBS. This allows for a more realistic and fair comparison, accounting both for advantages and drawbacks of the two different bandwidth management approaches. In Fig. 10, the achievable rate of the two schemes for perfect CSIT and $\beta = 4$ is presented. MU-VFDM shows a clear advantage in medium and high SNR regimes in terms of overall sum-rate of the two-tiered network, and the loss in the low SNR is very small if compared to the bandwidth partitioning based scheme. This result motivates a further comparison, when only an imperfect CSIT is available. In Fig. 11, we can see that MU-VFDM performs slightly worse if compared to the previous case, even if the overall sum-rate of the two-tiered network is still higher for the medium to high SNR regime if compared to reference scheme. Due to the nature of the cascaded precoder a bad channel estimation deteriorates the performance especially for low SNR values but, on the other hand, quite remarkably the advantage at high SNR is evident and promising. Therefore, MU-VFDM is able to exploit efficiently the higher multiplexing gain at the expense of a slightly worse performance for low SNR, for both CSIT assumptions.

## V. Conclusion

In this work, we presented a DSA cognitive overlay technique, called MU-VFDM, that allows the deployment of SBSs inside the coverage area of a preexisting MBS. We focused on the coexistence over the same bandwidth between a downlink LTE MBS and a SBS system, to illustrate both the feasibility and the performance of MU-VFDM. We have shown that, by increasing the number of SBSs, and therefore the dimensionality of the problem, the overall sum-rate of the two-tiered network can be enhanced. The network MIMO assumption made a potentially interference limited system become a MIMO-BC. Thanks to this fact, several linear precoding techniques involving cooperation between transmitters have been taken into account, and the inherent dimensionality constraint due to the structure of the precoder $\mathbf{E}$ has been identified. The search for a performing scheme brought us to the proposed flexible RIBF based approach presented in Sec. III-D. Increasing the number of transmit dimensions, while

keeping the receiver layout, is a viable way to design a system that overcomes the dimensionality problem and achieves relevant performance in terms of sum-rate. Such a system design, can be parameterized either by extra antenna installation, denser SBS deployment or a flexible combination of both. The relaxation of the perfect CSIT assumption at the SBSs results in rate loss experienced by both systems, due to the imperfectly devised precoder. The best compromise between training and data symbols has been investigated, for various SNR values, as well as the best performing strategy to deploy a dense network for the imperfect CSIT case. Finally, a comparison with state-of-the-art techniques has shown a remarkable advantage of the proposed technique for medium and high SNR values both for the perfect and imperfect CSIT case. The results presented herein reinforce our previous findings and confirm that MU-VFDM can be used to deploy SBSs and MBS coexisting inside the same coverage area, sharing the same band.

The analysis of the performance of this scheme under limited backhaul capacity assumption is matter of our future research, along with the impact of a partial cooperation between the SBSs. Moreover, we will move from a fully coordinated to a clustered network MIMO case, to find different and more practically implementable ways to manage the co-tier interference while guaranteeing the cross-tier interference nulling.

## REFERENCES


[1] J. Hoydis, M. Kobayashi, and M. Debbah. Green small-cell networks. *IEEE Vehicular Technology Magazine*, 6(1):37–43, 2011.

[2] M. Andrews, V. Capdevielle, A. Feki, and P. Gupta. Autonomous spectrum sharing for mixed LTE femto and macro cells deployments. In *2010 INFOCOM IEEE Conference on Computer Communications Workshops*, 2010.

[3] J. D. Hobby and H. Claussen. Deployment options for femtocells and their impact on existing macrocellular networks. *Bell Labs Technical Journal*, 13:145–160, 2009.

[4] VR Cadambe and SA Jafar. Interference Alignment and Degrees of Freedom of the $K$-User Interference Channel. *IEEE Transactions on Information Theory*, 54(8):3425–3441, 2008.

[5] R. Bhagavatula and R.W. Heath. Adaptive limited feedback for sum-rate maximizing beamforming in cooperative multicell systems. *IEEE Transactions on Signal Processing*, 59(2):800–811, 2011.

[6] S.M Perlaza, N. Fawaz, S. Lasaulce, and M. Debbah. From Spectrum Pooling to Space Pooling: Opportunistic Interference Alignment in MIMO Cognitive Networks. *IEEE Transactions on Signal Processing*, 58(7):3728–3741, 2010.

[7] W. Zhang and U. Mitra. Spectrum shaping: A new perspective on cognitive radio (part I): Coexistence with coded legacy transmission. *IEEE Transactions on Communications*, 58(6):1857–1867, 2010.

[8] S. Akoum, M. Zwingelstein-Colin, Heath R.W., and M. Debbah. Cognitive cooperation for the downlink of frequency reuse small cells. In *2nd International Workshop on Cognitive Information Processing*, 2010.

[9] J. Mitola. *Cognitive Radio An Integrated Agent Architecture for Software Defined Radio*. PhD thesis, Royal Institute of Technology (KTH), May 2000.

[10] *3GPP TR 25.814, Physical Layer Aspects for Evolved UTRA, v.2.0.0.* 3GPP, 2006.

[11] S. Shim, J.S. Kwak, R.W. Heath Jr., and J.G. Andrews. Block diagonalization for multi-user MIMO with other-cell interference. *IEEE Transactions on Wireless Communications*, 7(7):2671–2681, 2008.

[12] J. Wang, F. Adachi, and X. Xia. Coordinated and distributed MIMO. *IEEE Wireless Communications Magazine*, 17(3):24–25, 2010.

[13] A. Goldsmith, S.A. Jafar, I. Maric, and S. Srinivasa. Breaking spectrum gridlock with cognitive radios: An information theoretic perspective. *Proceedings of the IEEE*, 97(5):894–914, 2009.

[14] M.H.M. Costa. Writing on dirty paper. *IEEE Transactions on Information Theory*, 29(3):439–441, 1983.

[15] F. Jr. Ayres. *Theory and Problems of Matrices*. Mcgraw-Hill, 1967.

[16] L.S. Cardoso, M. Kobayashi, Ø. Ryan, and M. Debbah. Vandermonde frequency division multiplexing for cognitive radio. In *Proceedings of the 9th IEEE Workshop on Signal Processing Advances in Wireless Communications*, 2008.

[17] G. Caire and S. Shamai. On the achievable throughput of a multiantenna gaussian broadcast channel. *IEEE Transactions on Information Theory*, 49(7):1691–1706, 2003.

[18] A. Goldsmith. *Wireless communications*. 2005.

[19] Q.H. Spencer, A.L. Swindlehurst, and M. Haardt. Zero-forcing methods for downlink spatial multiplexing in multiuser MIMO channels. *IEEE Transactions on Signal Processing*, 52(2):461–471, 2004.

[20] C.B. Peel, B.M. Hochwald, and A.L. Swindlehurst. A vector-perturbation technique for near-capacity multiantenna multiuser communication (part I): channel inversion and regularization. *IEEE Transactions on Communications*, 53(1):195–202, 2005.

[21] R. de Miguel and R.R. Muller. Vector precoding for a single-user MIMO channel: Matched filter vs. distributed antenna detection. In *First International Symposium on Applied Sciences on Biomedical and Communication Technologies*, 2008.

[22] P. Viswanath, Tse D., and Laroia R. Opportunistic beamforming using dumb antennas. *IEEE Transactions on Information Theory*, 48(6):1277–1294, 2002.

[23] M. Sharif and B. Hassibi. On the capacity of MIMO broadcast channel with partial side information. *IEEE Transactions on Information Theory*, 51(2):506–522, 2005.

[24] V. Stankovic and M. Haardt. Multi-user MIMO downlink precoding for users with multiple antennas. In *Proc. 12-th Meeting of the Wireless World Research Forum*, 2004.

[25] V. Stankovic and M. Haardt. Generalized design of multi-user MIMO precoding matrices. *IEEE Transactions on Wireless Communications*, 7(3):953–961, 2008.

[26] T. Yoo and A. Goldsmith. On the optimality of multiantenna broadcast scheduling using zero-forcing beamforming. *IEEE Journal on Selected Areas in Communications*, 24(3):528–541, 2006.

[27] G. Dimic and N. Sidiropoulos. On downlink beamforming with greedy user selection: Performance analysis and simple new algorithm. *IEEE Transactions on Signal Processing*, 53(10):3857–3868, 2005.

[28] D. Tse and P. Viswanath. *Fundamentals of wireless communication*. Cambridge University Press, 2005.

[29] F. Boccardi, F. Tosato, and G. Caire. Precoding schemes for the MIMO-GBC. In *International Zurich Seminar on Communication*, 2006.

[30] B. Hassibi and B. Hochwald. How much training is needed in multiple-antenna wireless links? *IEEE Transactions on Information Theory*, 49(4):951–963, 2003.

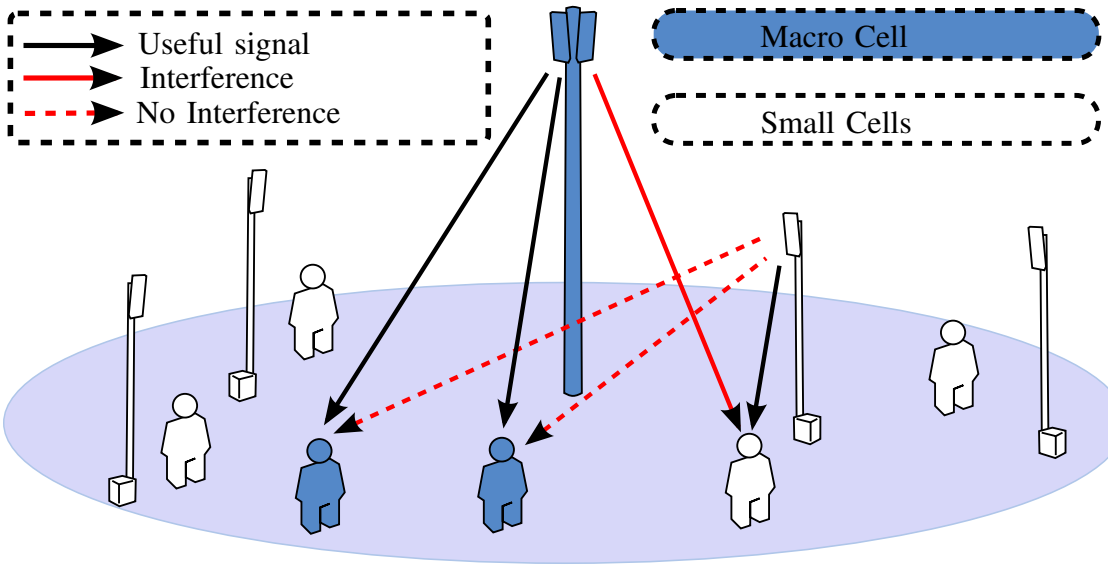



Figure 1. MU-VFDM downlink model, two-tiered network

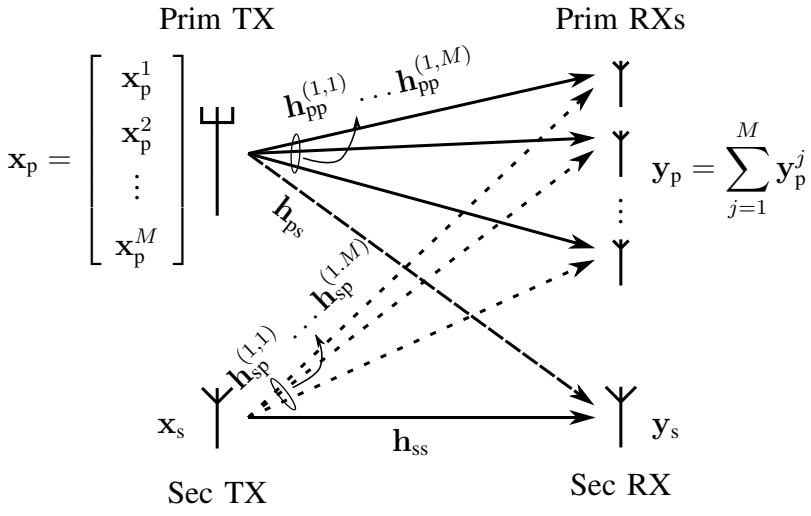



Figure 2. OFDMA downlink interference channel model, single SBS

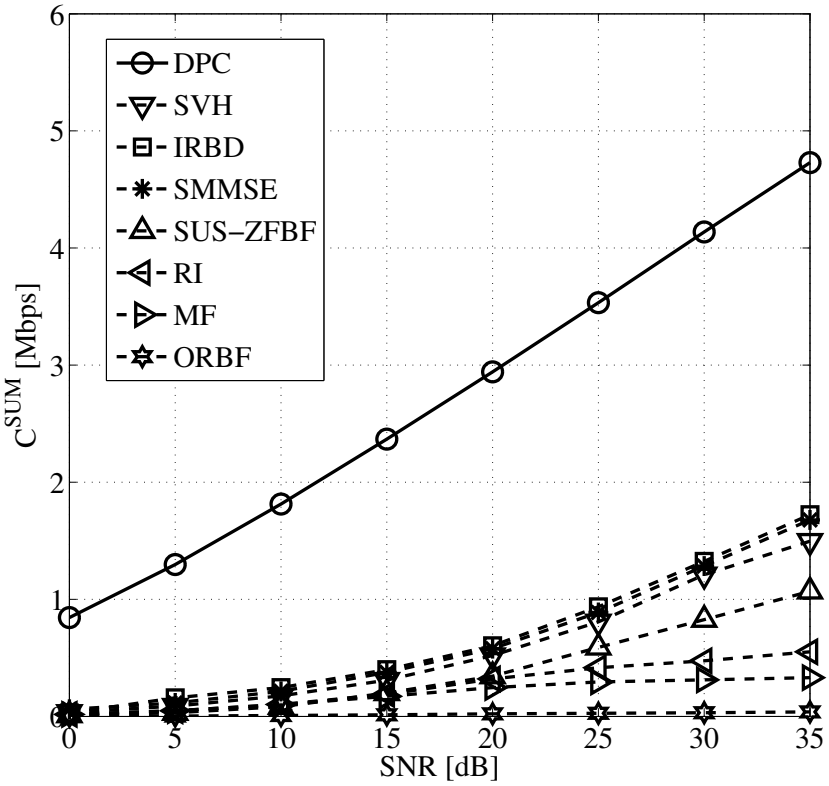



Figure 3. Rate of the SBSs for different transmit schemes, $K = 3$ ($N = 128, L = 32$ and bandwidth of 1.92 Mhz)

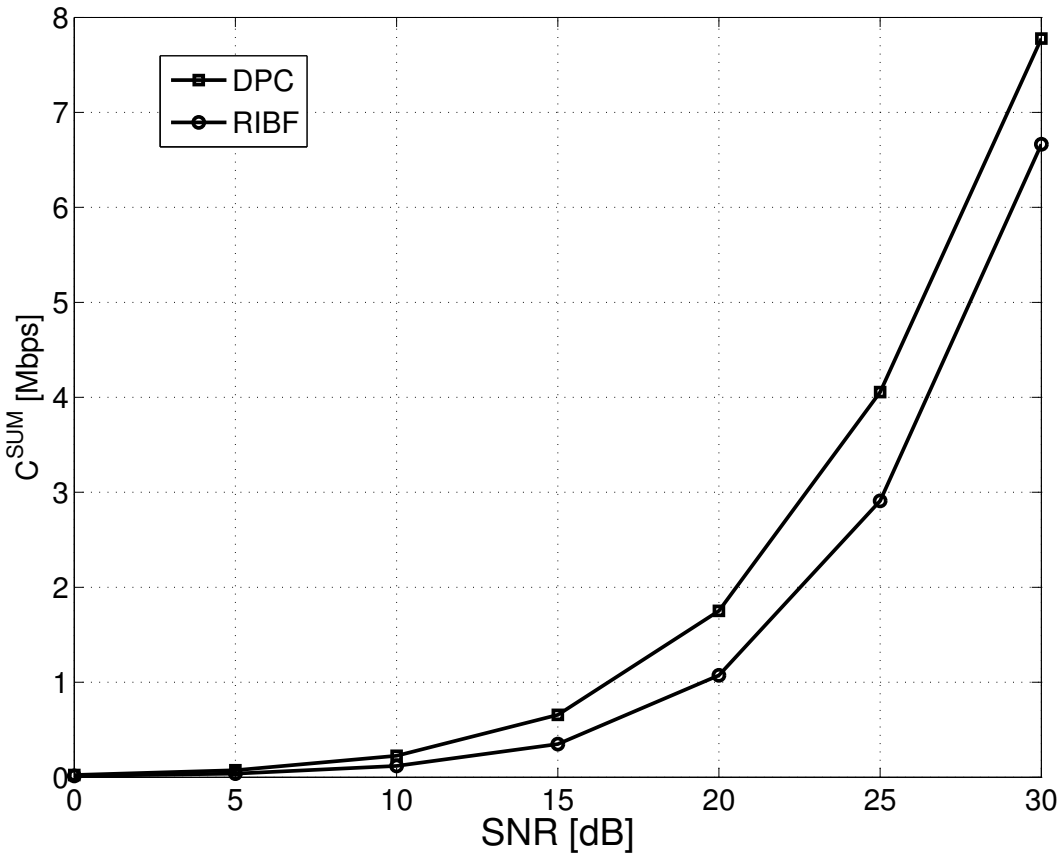



Figure 4. Achievable rate of the SBSs with the RIBF flexible network solution, $K = 3$, $\beta = 3$ ($N = 128, L = 32$ and bandwidth of 1.92 Mhz)

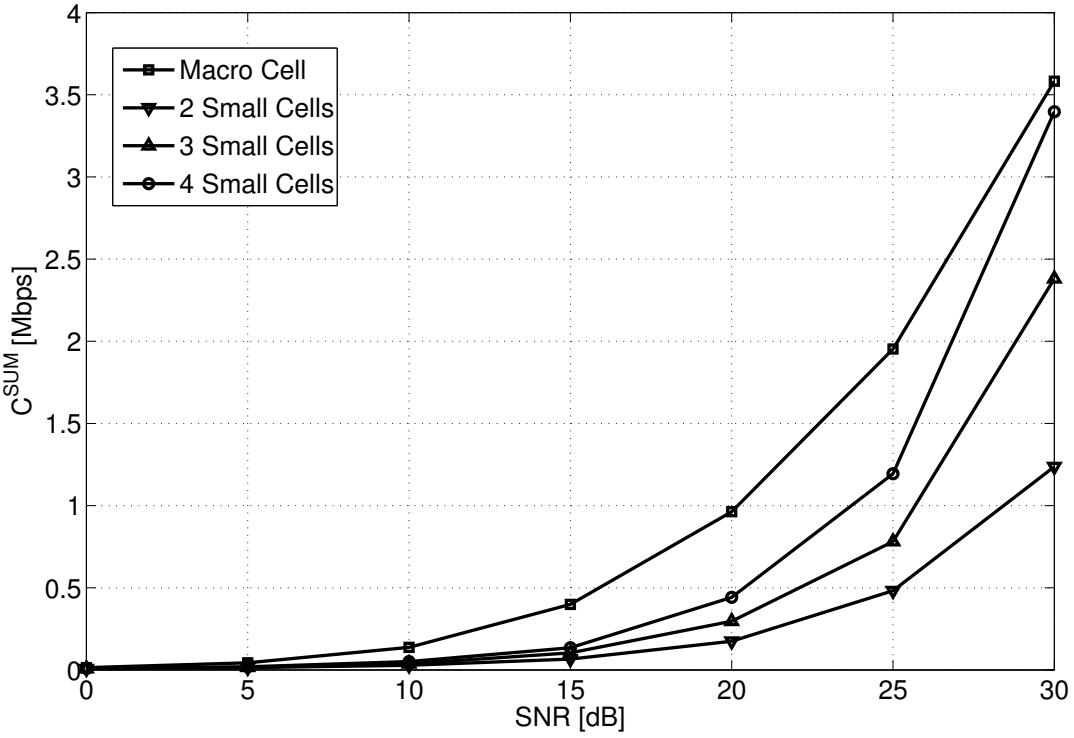



Figure 5. Rate of the SBSs with the RIBF flexible network solution for different numbers of small cells, $\beta = 2$, ($N = 128$, $L = 32$ and bandwidth of 1.92 Mhz)

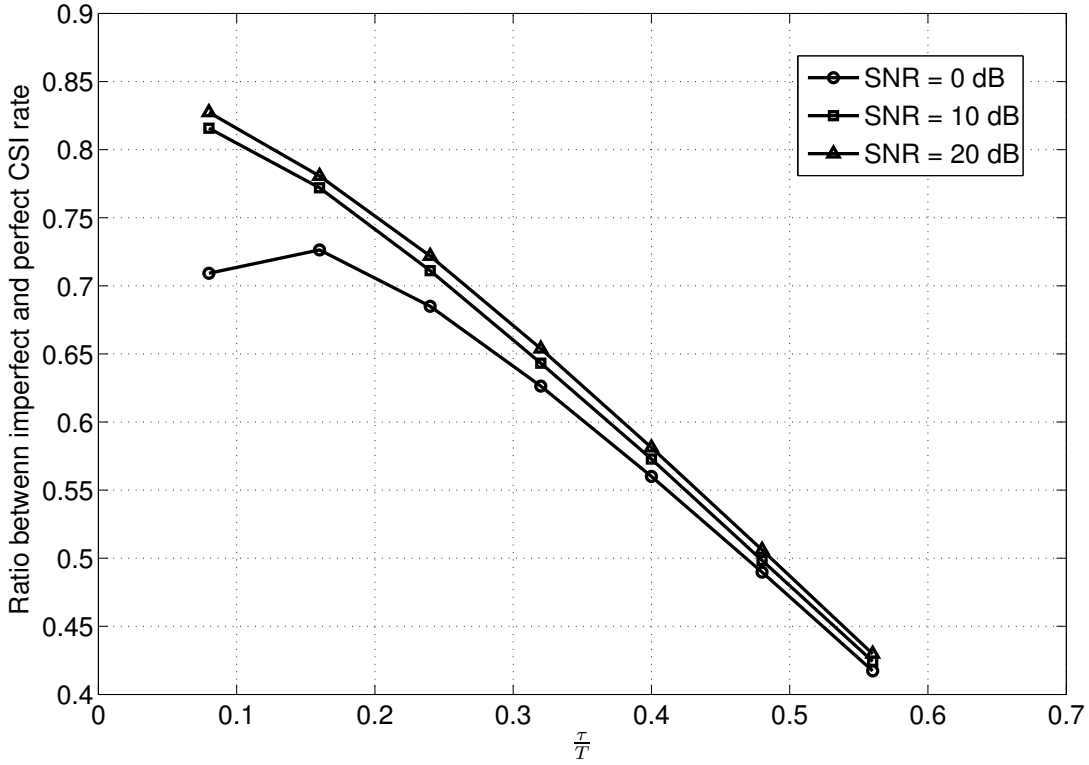



Figure 6. Macro cell performance with imperfect CSIT, $K = 3$, $\beta = 1$, ($N = 24, L = 6$ and bandwidth of 0.48 Mhz)

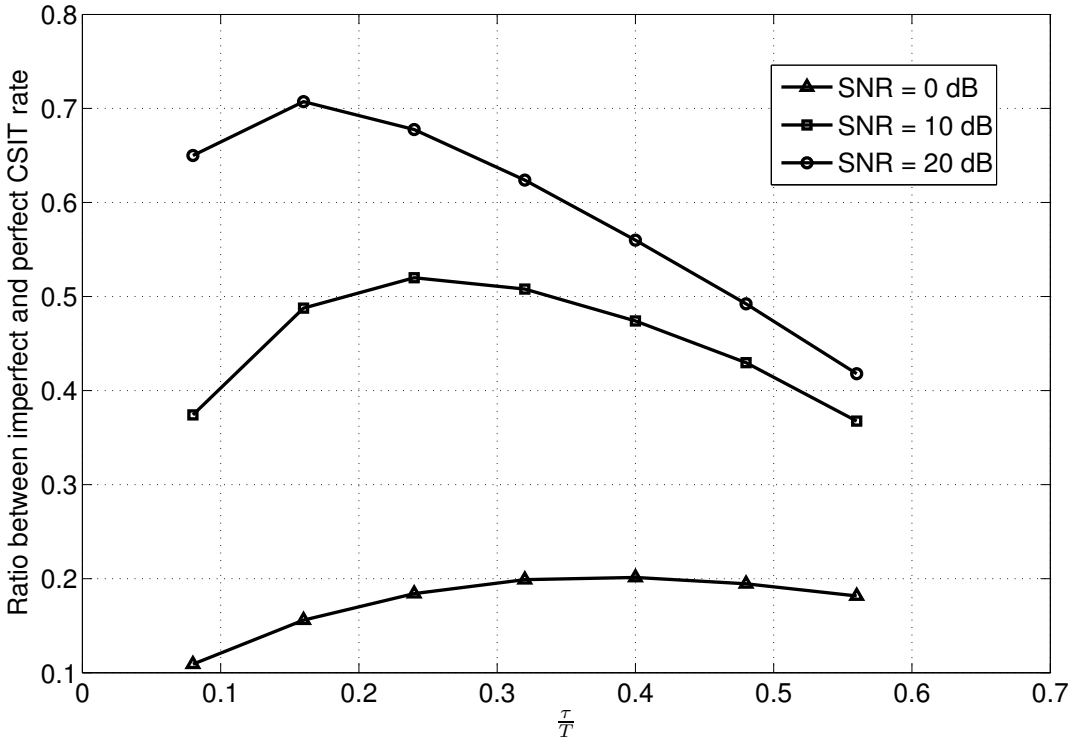



Figure 7. SBSs performance with imperfect CSIT, $K = 3$, $\beta = 1$, ($N = 24, L = 6$ and bandwidth of 0.48 Mhz)

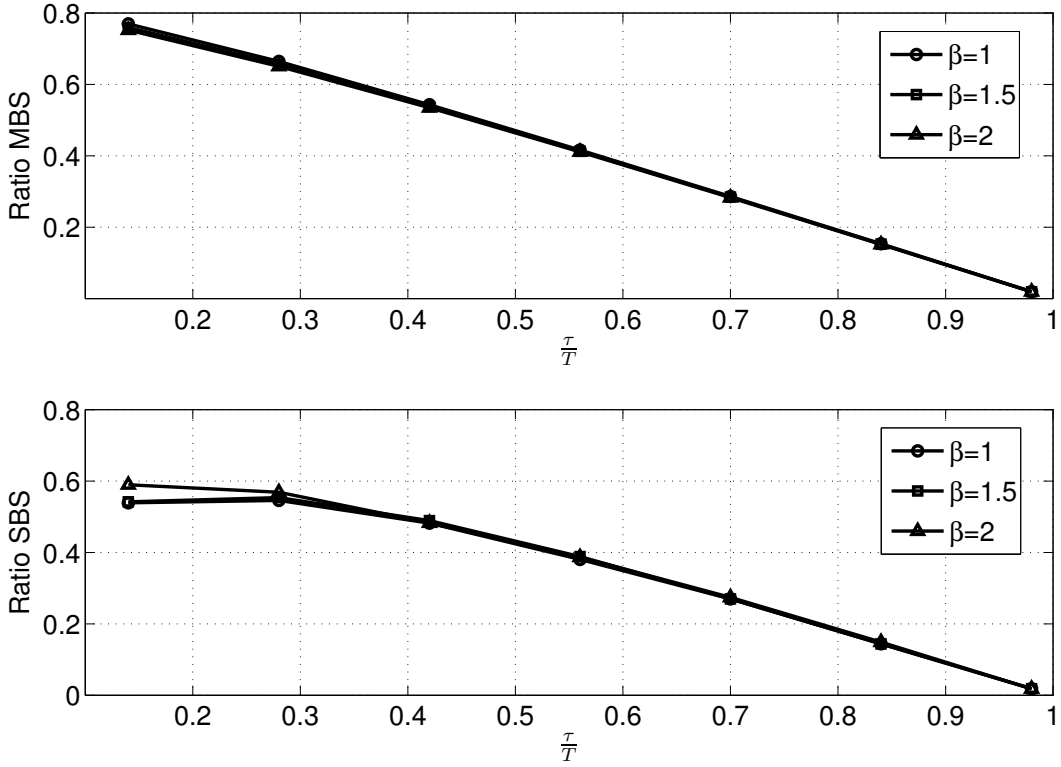



Figure 8. Ratio between the rate obtained with imperfect CSIT and the rate obtained with perfect CSIT for macro cell and small cell system as $\beta$ changes, and $K = 3$ ($N = 24, L = 6$ and bandwidth of 0.48 Mhz).

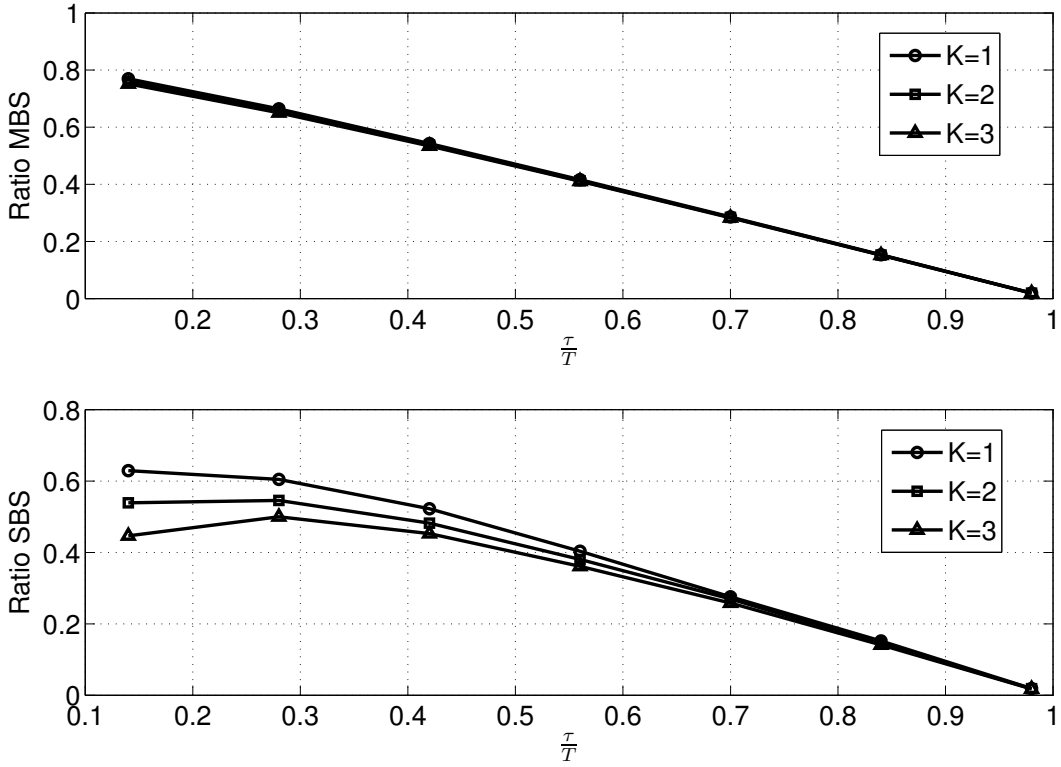



Figure 9. Ratio between the rate obtained with imperfect CSIT and the rate obtained with perfect CSIT for macro cell and small cell system as $K$ changes, and $\beta = 1$ ($N = 24, L = 6$ and bandwidth of 0.48 Mhz).

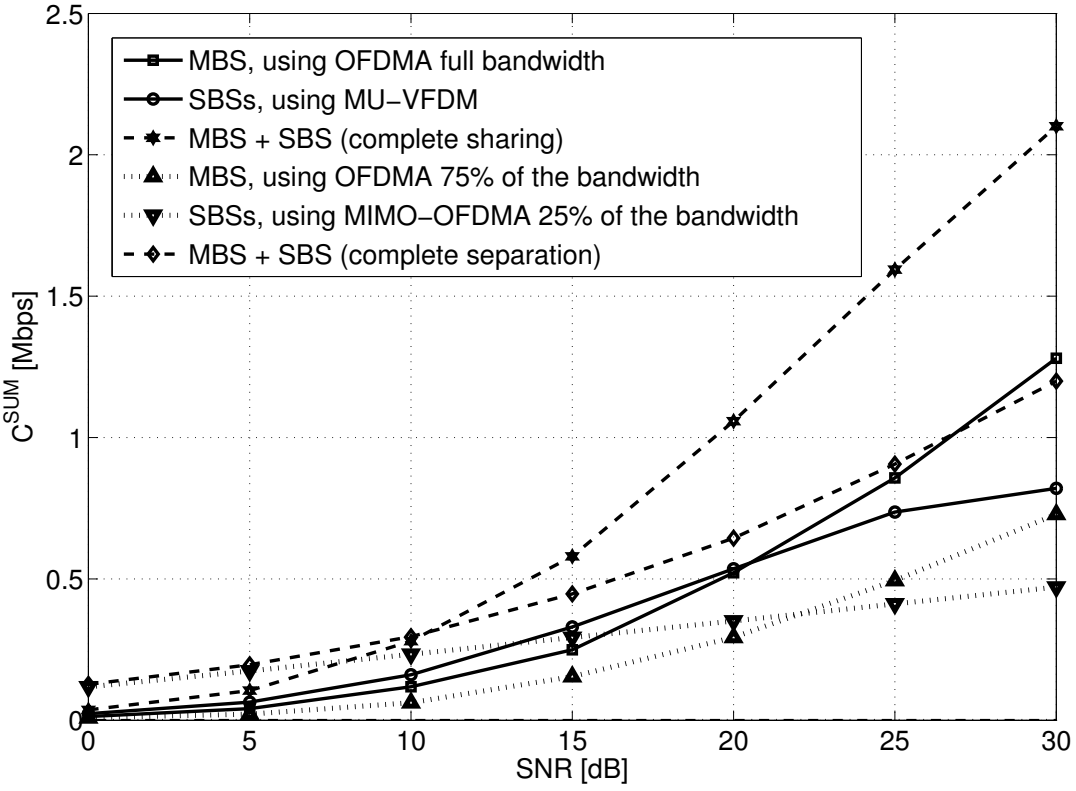



Figure 10. Achievable Rate of a two-tiered network, $K = 2$, $\beta = 4$, ($N = 24, L = 6$ and bandwidth of 0.48 Mhz). Perfect CSIT

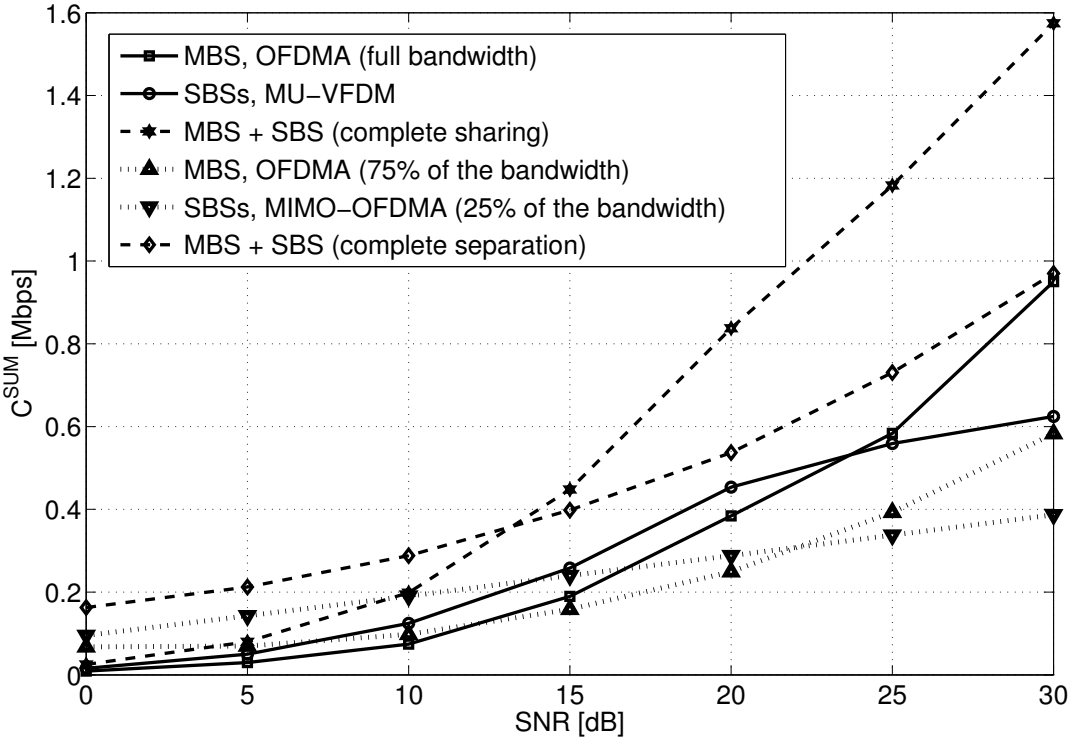



Figure 11. Achievable Rate of a two-tiered network, $K = 2$, $\beta = 4$, ($N = 24, L = 6$ and bandwidth of 0.48 Mhz. Imperfect CSIT